

Pattern Analogies

Learning to Perform Programmatic Image Edits by Analogy

Supplementary

Anonymous CVPR submission

Paper ID 1268

001 **1. Introduction**

002 In this document, we present additional details regarding
003 our system. First, we provide a brief overview of the videos
004 included in the supplemental material. Next, in section 3,
005 we provide details of the proposed Domain Specific Lan-
006 guage (DSL), SPLITWEAVE, including the design of the
007 two pattern-style specific program samplers. Section 5 pro-
008 vides additional details regarding *Analogical Quartet Sam-*
009 *pling*, detailing the *programmatic* pattern edits employed.
010 This is followed by details of our test dataset and the three
011 applications enabled by our approach in Section 6. Finally,
012 Sections 7, 8, 9 presents additional experiments and results,
013 including qualitative examples and failure cases. The code
014 for our system — the DSL, program samplers, and model
015 training — will be open sourced if and when the paper is
016 acceptance.

017 **2. Video Results**

018 We provide the following videos in the supplemental mate-
019 rials:

- 020 1. A video titled `editing.mp4` which demonstrates the
021 use of SPLITWEAVE for editing real-world patterns
022 with simple pattern analogies.
- 023 2. A video titled `pattern_animation.mp4` which
024 presents our results for pattern animation transfer.
025 Please refer to section 6.2 for more details on trans-
026 ferring pattern animations.

027 **3. A language for visual patterns**

028 In the main paper, we introduced SPLITWEAVE, a DSL de-
029 signed for creating visual patterns. As described previously,
030 we use SPLITWEAVE to (a) generate a large dataset of high-
031 quality synthetic patterns for training an analogical editor
032 and (b) to define parametric analogy pairs (A, A') at test-
033 time to guide transformation in target pattern B . Further,
034 we constructed two custom SPLITWEAVE program sam-
035 plers which aid the sampling of high-quality synthetic pat-

terns in two domains, namely *Motif Tiling Patterns* (MTP),
and *Split Filling Patterns* (SFP). 036 037

SPLITWEAVE is designed specifically for generating
patterns that exhibit structured partitioning of a 2D canvas.
Programs in SPLITWEAVE define a process to map each
spatial location on the canvas to an RGBA value, resulting
in a visual pattern. This process is achieved through two
core mappings: (1) spatial locations (x, y) are first mapped
to 2D UV coordinates and (2) UV coordinates are then
mapped to outputs such as RGBA values or other signals.
SPLITWEAVE provides operators to abstract and simplify
these mappings. 038 039 040 041 042 043 044 045 046 047

3.1. $UVExpr$ and $SEExpr$ 048

$UVExpr$ and $SEExpr$ are the two key types of expressions
used in SPLITWEAVE programs to define these mappings: 049 050

$UVExpr$ A $UVExpr$ defines a function 051

$$UVExpr : \mathbb{R}^2 \rightarrow \mathbb{R}^2, \quad 052$$

which maps each spatial location (x, y) on the canvas to
a corresponding UV coordinate (u, v) . This provides a
spatial framework for pattern generation, enabling opera-
tions such as distortions, tiling, or structured partitioning
(e.g., `BrickSplit`, `HexagonalSplit`). Evaluating a
 $UVExpr$ generates a UV grid which serves as the basis for
further evaluating $SEExpr$ s. 053 054 055 056 057 058 059

$SEExpr$ A $SEExpr$ defines a function 060

$$SEExpr : \mathbb{R}^2 \rightarrow \mathbb{R}^N, \quad 061$$

which maps each UV coordinate $(u, v) \in \mathbb{R}^2$ to an N -
dimensional output. The value of N depends on the type of
output being generated. $SEExpr$ s that evaluate to 4-channel
outputs ($N = 4$) are typically used to generate RGBA
canvases. Alternatively, $SEExpr$ s which evaluate to single-
channel outputs ($N = 1$) are used to generate single-channel 062 063 064 065 066 067

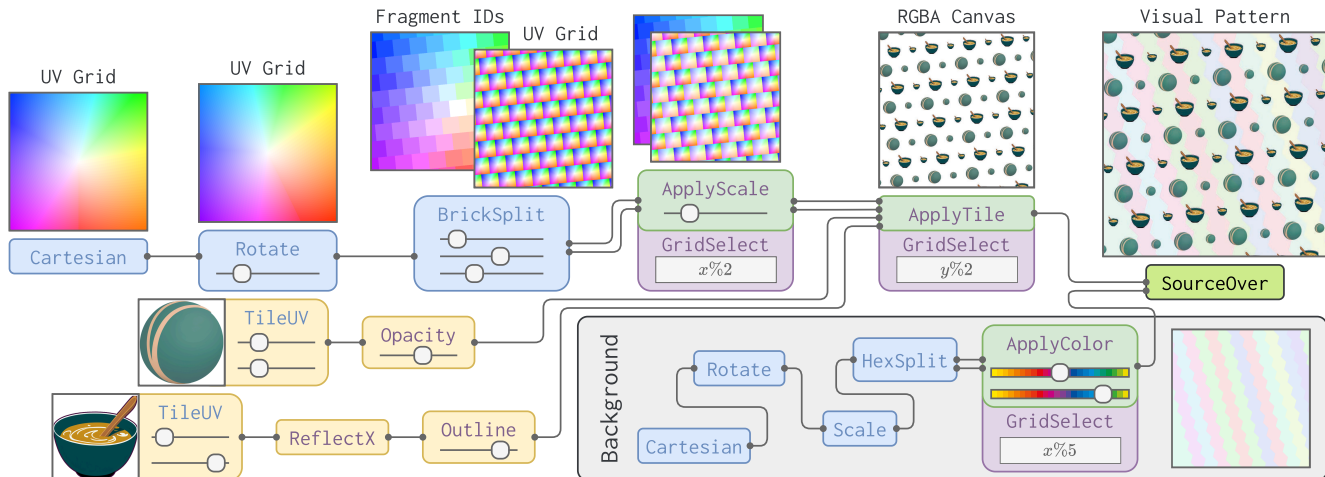


Figure 1. **Program evaluation** We illustrate the evaluation of a SPLITWEAVE program. SPLITWEAVE is used to create directed acyclic graphs representing data flow between different operators. The *UV Grid Operators* are used to define $UVExprs$, which map spatial coordinate to UV grids. *Signal Operators* are used to define $SEExprs$ which map UV-Grids to single or multi-channel spatial maps (such as RGBA canvases). *Spatially Varying Operators* take inputs such as UV-Grids and Fragment Ids to apply spatially varying transforms. Finally, *Utility Operators* perform tasks such as composing multiple RGBA canvases together.

068 buffers used to represent spatial masks, distortion fields, or
069 other intermediate signals.

070 $UVExprs$ are primarily used to generate structured parti-
071 tions of the canvas through partitioning operators (e.g.,
072 *BrickSplit*). Evaluating these operators produce not only
073 a corresponding UV grid, but also a **fragment ID buffer**,
074 where each spatial location is assigned a fragment identi-
075 fier corresponding to its partition. As operators are com-
076 posed, the fragment ID buffers are updated and stacked, en-
077 abling hierarchical partitioning and fragment-aware trans-
078 formations. This mechanism is critical for supporting *Spa-*
079 *tially Varying Transformations*, used in *Motif Tiling Pat-*
080 *terns* (MTP), where operations vary based on partitioning,
081 and *Fragment Grouping*, essential for *Split-Filling Pat-*
082 *terns* (SFP), where fragments are grouped together for applying
083 color fills.

084 $SEExprs$ typically contain analytical functions defining
085 SVG objects, such as 2D circles, Bezier curves etc, and
086 Texture-Mapping operators, which map UV coordinates
087 to samples on pre-defined 2D maps. Texture mapping op-
088 erators are primarily used for mapping RGBA tiles on UV
089 grids. Evaluating $SEExpr$ on different UV-grids results in
090 different outputs. These outputs are used to generate RGBA
091 canvases or auxiliary data buffers for generating the visual
092 pattern image.

093 3.2. Operator Categories

094 SPLITWEAVE provides four broad categories of operators
095 to support the construction of $UVExprs$, $SEExprs$, and their
096 transformations:

097 1. ~ 50 *UV Grid Operators*: Used to define $UVExprs$.

098 2. ~ 70 *Signal Operators*: Used to define $SEExprs$.

099 3. 10 *Spatially Varying Operators*: Used to define trans-
100 formations in a partition-aware manner using frag-
101 ment IDs (e.g., resizing alternate rows or applying per-
102 fragment coloring).

103 4. *Utility Operators*: Used for remaining purposes such
104 as combining multiple canvases (*SourceOver*) or gener-
105 ating auxiliary spatial signals used in fragment-
106 aware operations.

107 In Figure 1, we illustrate the evaluation of a
108 SPLITWEAVE program used to create a MTP pattern. This
109 program uses all the four different types of operators,
110 each associated with a separate color. To create the pat-
111 tern, we separately create a background canvas and a fore-
112 ground canvas. To create the foreground canvas, we first
113 convert the pixel-space canvas to a UV cartesian grid (\in
114 $[-1, 1]^2$) using *Cartesian*. This grid is subsequently
115 rotated using the *Rotate* operator. Next, by using the
116 *BrickSplit* operator, we create two outputs, a trans-
117 formed UV-grid, which now consists of brick-style spatial
118 partitions, and a 2D fragment-ID buffer containing integers
119 that corresponds to fragment IDs. Using the fragment-ID
120 buffer, we apply spatially-varying scaling to decrease the
121 size of tiles in alternate columns. This is followed by a
122 *ApplyTile* operator to create the foreground canvas. In-
123 ternally, *ApplyTile* evaluates the $SEExprs$ corresponding
124 to each tile on the transformed UV-grid, and merges alter-
125 nate rows of the resulting two RGBA canvases using the
126 fragment-ids from *BrickSplit*. A similar process is fol-
127 lowed for the background to obtain the background canvas.

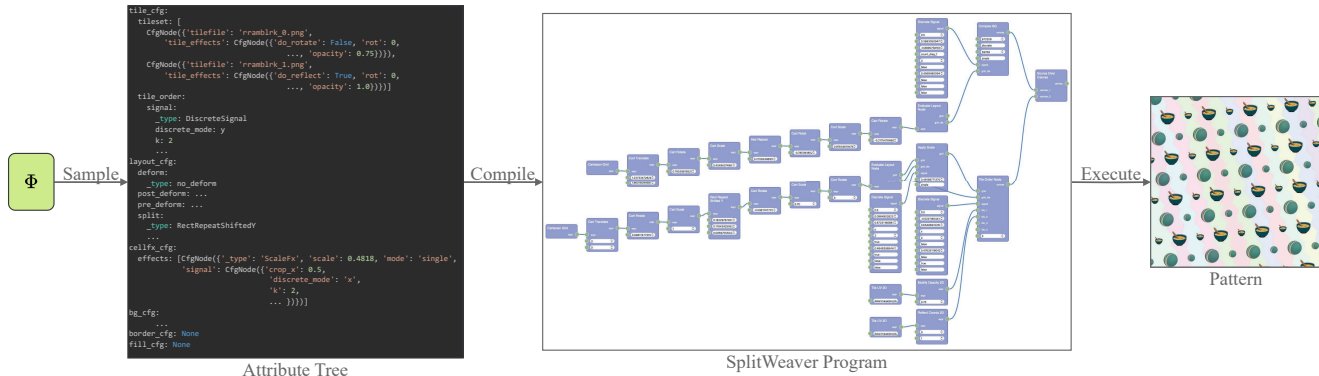


Figure 2. Our Custom program samplers Φ generates attribute trees AT , a hierarchical data structure that encodes patterns structure specification. The attribute trees are then compiled into SPLITWEAVE programs. Finally, we generate visual patterns by evaluating SPLITWEAVE program. The use of Φ and AT help generate high-quality synthetic patterns.

128 Finally, we combine the background and foreground with
129 the `SourceOver` operator to obtain the final MTP pattern.

130 3.3. Implementation

131 SPLITWEAVE is implemented in Python, making it acces-
132 sible to a wide range of users, including those with limited
133 programming experience. This lowers the learning curve
134 for novice users and facilitates integration with emerging
135 tools, such as large language models (LLMs), for program-
136 matic generation and manipulation of visual patterns. The
137 core operators in SPLITWEAVE are implemented using Py-
138 Torch [9], which allows many of the operators to be auto-
139 matically differentiable. This opens up exciting possibilities
140 for future work in using automatic differentiation for visual
141 program inference, enabling the recovery of programmatic
142 structures directly from visual patterns.

143 We have also developed a front-end application using
144 `Rete.js` [3] to support visual programming with
145 SPLITWEAVE. This tool simplifies the creation and man-
146 ipulation of SPLITWEAVE programs by providing an intu-
147 itive, node-based interface. Manipulation of SPLITWEAVE
148 programs using this interface is demonstrated in the supple-
149 mental videos. Currently implemented as a proof of concep-
150 t, it is primarily intended for inspecting SPLITWEAVE
151 programs and performing parametric analogical edits on
152 real-world patterns. Future work will focus on refining the
153 application to make it more user-friendly and suitable for
154 broader usage. We hope that SPLITWEAVE serves as a step-
155 ping stone for further research in visual pattern generation
156 and manipulation, inspiring new methodologies and appli-
157 cations in this domain.

158 4. Custom Program Samplers

159 As discussed in the main paper, random sampling of the
160 SPLITWEAVE grammar often produces poor-quality pat-
161 terns that are incoherent or irrelevant for training. To ad-

dress this limitation, we construct custom program samplers
designed to generate high-quality SPLITWEAVE programs
through a structured, hierarchical process.

The custom program samplers work by generating an *at-tribute tree*, a hierarchical data structure that encodes the specification for a pattern. This attribute tree is then compiled into a valid SPLITWEAVE program, which, when executed, produces the final visual pattern. The pipeline can be formalized as:

$$\Phi \xrightarrow{\text{Sample}} AT \xrightarrow{\text{Compile}} P_{SW} \xrightarrow{\text{Execute}} \text{Pattern},$$

where Φ is a high-level process specification that defines the abstract structure of the pattern, AT is the attribute tree that instantiates this structure with specific parameters, and the resulting SPLITWEAVE program, represented as P_{SW} , defines the procedural steps to produce the pattern. Figure 2 illustrates this workflow with an example, showing the attribute tree, its compilation into a SPLITWEAVE program, and the resulting visual pattern.

The attribute tree AT is constructed by first designing an abstract process specification Φ that represents the steps involved in creating a pattern. For example, in Motif Tiling Patterns (MTP), Φ includes stages such as sampling tiles, sampling layout parameters, and sampling effects like background elements. Each stage in Φ corresponds to a node or sub-tree in AT , where the nodes represent specific components, and the edges encode relationships or contextual parameters. To populate AT , we implement domain-specific random samplers for each node in the tree. These samplers generate valid and diverse configurations for their respective components. At the top level, a hierarchical sampler integrates these components to form a complete attribute tree. For instance, the MTP sampler samples specification for canvas partitioning, tiles and their transformations and spatially varying effects, combining them into a unified representation.

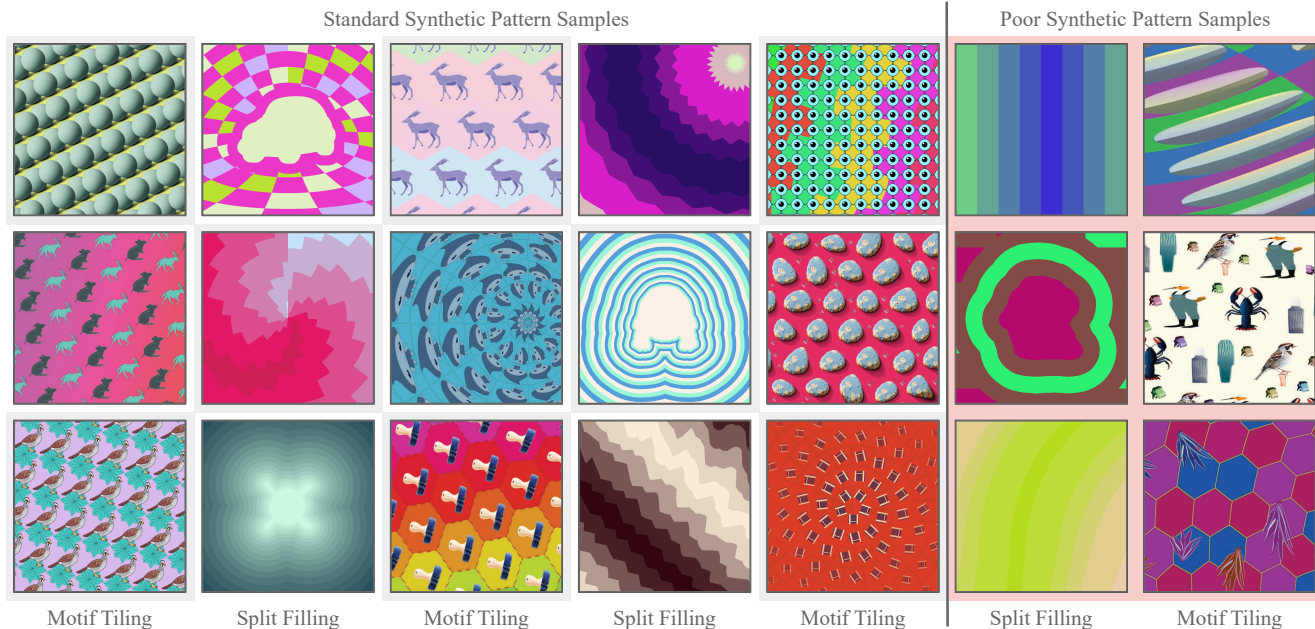


Figure 3. We present synthetic samples generated by our custom program samplers for two pattern styles, namely, Motif Tiling Patterns (MTP) and Split Filling Pattern (SFP). The custom program sampler can still produce poor quality patterns as depicted in the rightmost two columns.

197 The hierarchical nature of the attribute tree allows modular
 198 control over each component, enabling flexibility and
 199 extensibility. By sampling each node independently, the
 200 custom samplers ensure that the resulting patterns are both
 201 diverse and semantically meaningful, addressing the chal-
 202 lenges of random grammar sampling. Once the attribute
 203 tree AT is constructed, it is compiled into a SPLITWEAVE
 204 program. This compilation step translates the hierarchi-
 205 cal structure and parameters encoded in AT into valid
 206 SPLITWEAVE code, adhering to the syntax and semantics
 207 of the DSL. Executing the compiled SPLITWEAVE program
 208 produces the final visual pattern. This structured workflow
 209 provides a controlled and flexible framework for generat-
 210 ing patterns. The combination of a process-driven attribute
 211 tree design and creation of pattern style-specific samplers
 212 ensures the generation of high-quality visual patterns.

213 In figure 3, we present synthetic samples of both MTP
 214 and SFP styles generated by this process. We also show fail-
 215 ure cases in the two right-most columns. The custom sam-
 216 pler for MTP patterns sometimes generates samples with a
 217 high amount of stretching, too much visual complexity, or
 218 sparse tiling. Similarly, SFP pattern sampler can fail due
 219 to trivial grid partitioning, over-zooming, or poor random
 220 color section.

221 To create the MTP patterns we also generate a large
 222 dataset of 100,000 RGBA tiles. Earlier experiments with
 223 fewer tiles showed that having a diverse and large set of
 224 tiles is essential to generalize to ‘in-the-wild’ real-world

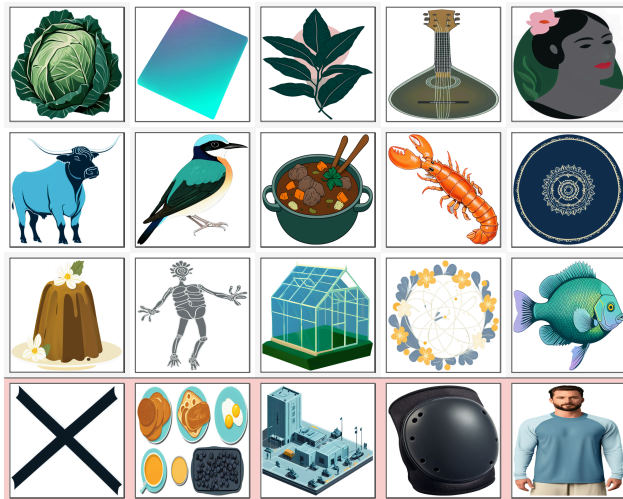


Figure 4. We generate tiles for MTP patterns using LayerDif-
 fuse [15]. We present both good quality tiles (top 3 rows)
 and poor quality tiles (bottom row).

225 patterns. To create tiles on a large variety of subjects, we
 226 first extract a subset of nouns from wordnet-synset [8].
 227 First, we prune the nouns by type (avoiding types such as
 228 ‘event’, ‘process’), followed by rejection based on keyword
 229 match (to avoid different forms of ‘bacteria’, ‘virus’ etc.).
 230 Finally, we use SigLIP [14] text-encoding of prompts in the
 231 form of ‘‘A photo of a/an \$item’’ to cluster the

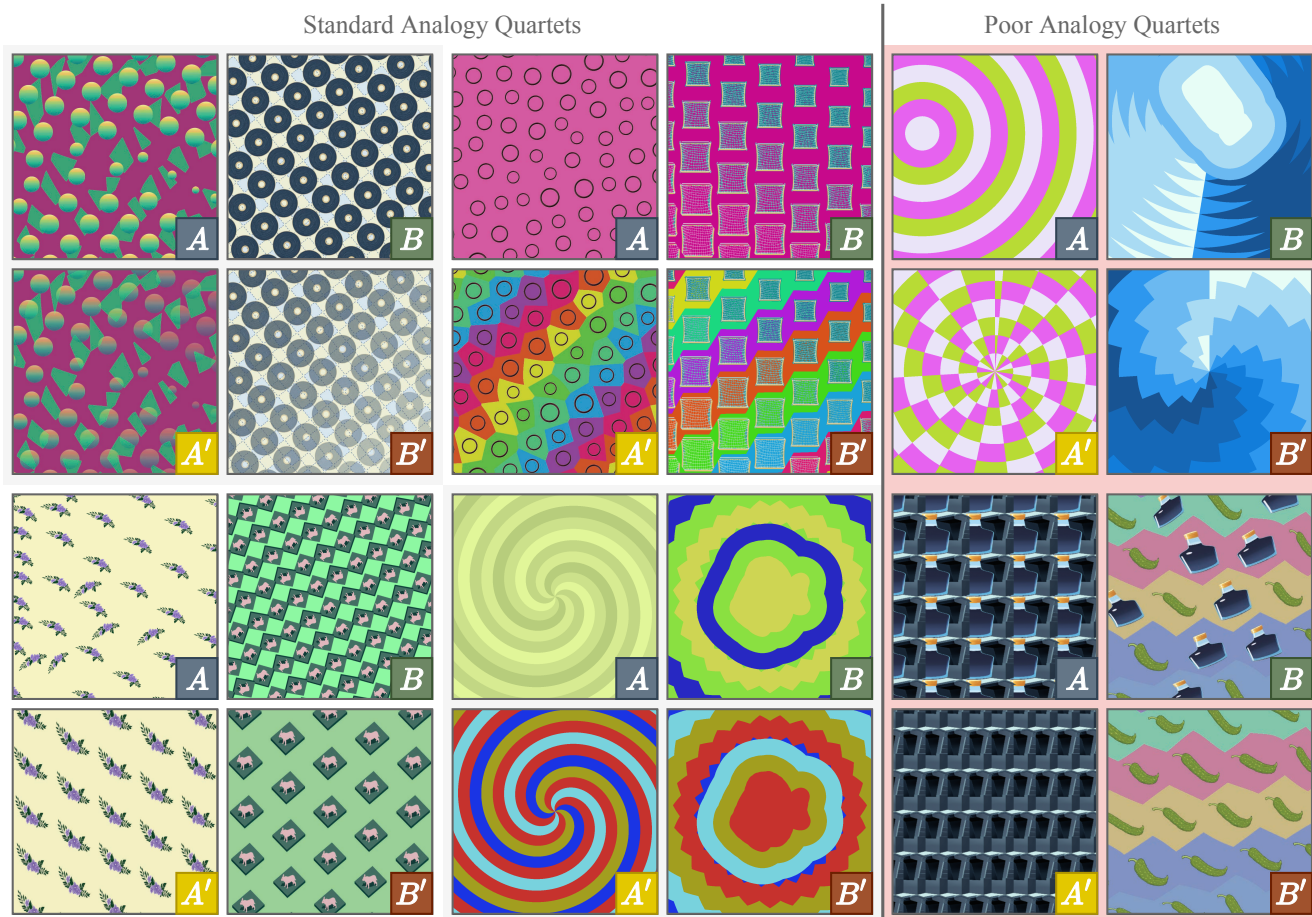


Figure 5. We present analogical quartets created using our approach. While many analogical quartets are of good quality, our synthetic sampling process can also result in poor quality quartets, as shown in the right-most column.

232 nouns and extract $\sim 10,000$ distinct nouns. These nouns
 233 are then used to create text-prompts using a template of the
 234 form ```A minimal $style $second_term of
 235 a $noun $minimalism on a $color_scheme
 236 background.``` where the variables such as `$style`
 237 and `$second_term` are filled with random samples from
 238 list of keywords. Then, we generate RGBA images for each
 239 prompt using LayerDiffuse [15], which generates images
 240 with alpha maps. Finally, tiles are created by extracting
 241 a tight bounding box subset of the generated image, with
 242 simple thresholds to reject samples in case of too high and
 243 too low complexity (measured using JPEG [13] compression).
 244 Figure 4 presents a few samples of tiles generated
 245 by this process. We note a few recurring failure cases: a)
 246 Extremely simple tiles, b) tiles with multiple objects, c)
 247 Tiles with poor cropping, and d) realistic rendering effects
 248 on tiles. Despite these flaws, a majority of the tiles seem to
 249 be useful, particularly to help to model avoid overfitting to
 250 training tiles.

5. Sampling Analogical Quartet

251
 252 In the main paper, we introduced analogical quartets
 253 (A, A', B, B') that are used to our train analogical editing
 254 model. These quartets are grounded in Structure Mapping
 255 Theory [6], which defines analogies as mappings of relational
 256 structure from a base to a target domain. The relation-
 257 ship R between program pairs $(z_A, z_{A'})$ and $(z_B, z_{B'})$
 258 remains consistent:

$$R(z_A, z_{A'}) = R(z_B, z_{B'}). \quad (1) \quad 259$$

260 Here, we provide additional details on how edits are
 261 defined, sampled, and applied to construct these quartets,
 262 along with examples and a discussion of failure cases.

263 Edits in our framework operate directly on the attribute
 264 tree AT , rather than on SPLITWEAVE programs. This ap-
 265 proach ensures semantic validity and allows for efficient re-
 266 sampling of components. Each edit targets a node just be-
 267 low the root of the tree, corresponding to high-level com-
 268 ponents in the pattern creation process. For Motif Tiling

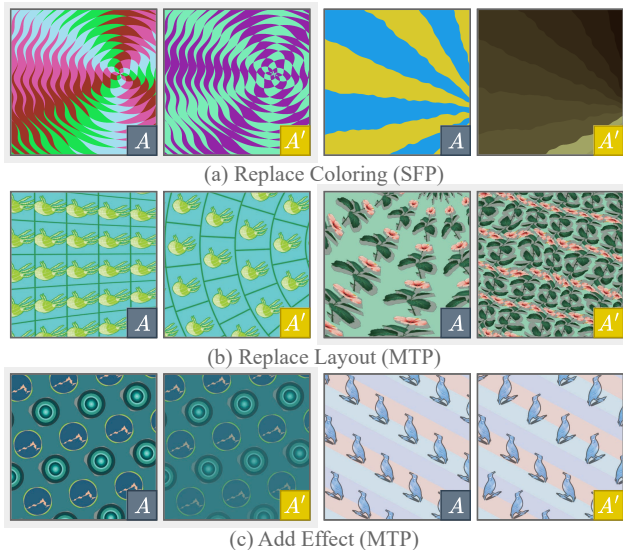


Figure 6. We present examples of editing synthetic patterns A with different edits to generate edited pattern A' .

Patterns (MTP), the editable components include:

1. *Tiles*: Add, remove, or replace tiles in the pattern.
2. *Layout*: Replace the layout structure.
3. *Cell Effects*: Add or remove specific spatially varying effects applied to cells.
4. *Background and Border*: Replace background or border styles.

For Split-Filling Patterns (SFP), the editable components include:

1. *Foreground Layout and Background Layout*: Replace the layout for either foreground, background or both elements.
2. *Fill Specifications*: Replace the specifications for filling regions.

Edits are applied by resampling or modifying nodes in the attribute tree. To perform a *replace* edit, the target node is resampled to produce a new specification, such as a new layout or tile configuration, and this new specification is used to create both A' and B' . To perform a *add* edit, a new node is created and inserted into the appropriate list (e.g., adding a tile or effect). Finally, to perform a *remove* edit, a node is added, and the order of the quartet is flipped (e.g., swapping $A \leftrightarrow A'$ and $B \leftrightarrow B'$). Applying random edits to randomly sampled pattern sets (A, B) can generate invalid new pattern (A', B') . Therefore, we instead first sample an edit e and, perform rejection sampling of (A, B) pairs to generate valid analogical quartets.

In Figure 6, we present some examples of pattern pairs generated by editing a pattern A to create A' , of both MTP and SFP styles. Figure 5 provides examples of generated



Figure 7. Our model enables users to mix aspects of different patterns to create novel patterns. In this example, The layout of X is mixed with the tiles of Y to generate the pattern Y' .

analogical quartets, demonstrating consistent transformations between (A, A') and (B, B') . Despite its robustness, our approach can encounter failure cases. For instance, despite the pattern programs satisfying equation 1, visually salient relation between (A, A') and (B, B') may not be analogical. Furthermore, sometimes (A, A') pair may not clearly demonstrate the desired change.

6. Additional Details

We now provide additional details regarding our test set consisting of real-world patterns, and

6.1. Test Set Creation

To evaluate our method, we created a test set by collecting 116 patterns from Adobe Stock. Based on visual inspection, we annotated desirable edits for 50 patterns in text. For each annotated edit, we manually constructed input analogies using SPLITWEAVE. These analogies were not always designed to be simple, as we aimed to test the model’s ability to interpret non-trivial analogies effectively. The test set, along with annotated edits, is included in the supplementary material.

6.2. Application: Pattern Mixing

The goal of pattern mixing is to transfer aspects of one real-world pattern X to another real-world pattern Y . This approach makes it easier to create novel variations of patterns and to transfer specific aspects of patterns that may not be present in our synthetic dataset. To achieve this, we construct an analogy pair (X, X') , which is used as input to edit Y . This sequential process, referred to as “chaining,” allows edits to build upon the outputs of previous steps.

Our model’s ability to use real-world patterns as analogy inputs enables chaining, which is critical for pattern mixing. This capability is attributed to the scale and diversity of the synthetic dataset used during training. Figure 7 illustrates this process for a pair (X, Y) where we mix the layout of X with the tiles of Y .

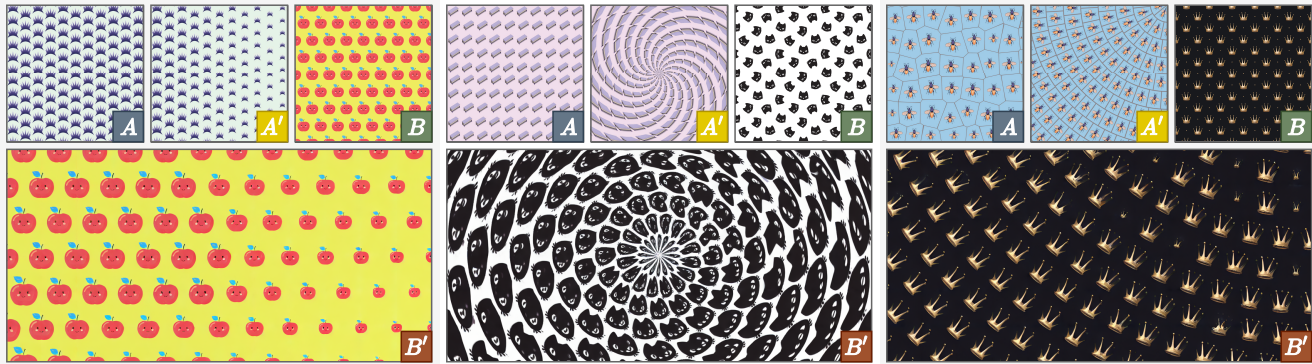


Figure 8. Our model can also be used to create wide canvases of non-stationary patterns by adapting MultiDiffusion [2] for spatially-conditioned generation. In these examples, we generate patterns of size 1536×1536 pixels and show a vertically centered crop.

334 6.3. Application: Pattern Animation

335 This application allows users to transfer an animations cre-
 336 ated using simple synthetic pattern A to real-world patterns
 337 B . Traditionally, such transfers require inferring the pro-
 338 gram for B and applying the animation to it. In contrast,
 339 with our method, users can automatically create analogy
 340 pairs from A 's animation sequence to generate correspond-
 341 ing variations in B . The user provides as input (A, \mathbf{A}') ,
 342 where \mathbf{A}' represents the frames of the animation, and a real-
 343 world pattern B . We then employ TRIFUSER to generate
 344 variations of B that correspond to analogy pairs created for
 345 each frame as follows:

$$346 \mathbf{B}' = \{B' = M(A, A', B) | A' \in \mathbf{A}'\}. \quad (2)$$

347 To ensure temporal consistency, for each frame, we fix
 348 the initial latent noise, generate $n = 5$ samples and se-
 349 lect the one with the lowest PSNR relative to the preced-
 350 ing frame. This approach avoids program inference and en-
 351 ables automated animation transfer. A demonstration video
 352 is provided in the supplementary material. In future, we
 353 hope to enforce stronger priors to improve temporal consis-
 354 tency.

355 6.4. Application: Wide Non-stationary Canvas

356 Visual patterns often need to adapt to varying resolutions,
 357 such as for use in presentations or posters. This is com-
 358 monly achieved for stationary patterns by making the pat-
 359 tern image seamlessly tile-able. In fact, images generated
 360 using convolution-based diffusion models can also be made
 361 seamlessly tile-able by employing circular padding in the
 362 convolution layers. However, no such solution exists for
 363 non-stationary patterns. We provide a novel solution by
 364 adapting Multi-Diffusion [2] to our settings.

365 Multi-Diffusion solves the task of generating large im-
 366 ages with diffusion models. This is achieved by first gen-
 367 erating model predictions on tiled crops of the canvas and

	Analogy data	DSIM (↓)	DISTS (↓)	LPIPS (↓)	SSIM (↑)
<i>LatentMod</i> CATEGORICAL	✗	0.242	0.320	0.613	0.502
<i>LatentMod</i> TOKENWISE	✗	0.307	0.333	0.581	0.500
<i>LatentMod</i> ANALOGICAL	✓	0.273	0.330	0.620	0.525

Table 1. We compare different variations of *LatentMod* baselines. We observe that none of the variations are suitable for performing precise *programmatic* edits, indicating the unsuitability of latent-arithmetic based analogical editing for precise structure editing.

using the average predicted noise across overlapping image
 crops at each denoising step. Applying this naively to our
 method fails as our model strongly depend on the condition-
 ing input (A, A^*, B) for generating B' , i.e., they have strong
 dependence on the spatial orientation of the conditioning
 embeddings. To circumvent this issue, we adapt multi-
 diffusion for our model by performing consistent cropping
 across analogy inputs (A, A^*, B) and the latent code of B^*
 during generation. This adaptation enables the generation
 of wide, non-stationary canvases. Figure 8 illustrates three
 examples generated using this method, where we generated
 wide canvases which are 1536×1536 pixels in size.

7. Quantitative Results

We now describe additional experiments conducted to fur-
 ther validate our system. First we discuss quantitative eval-
 uations in this section, followed by qualitative results in sec-
 tion 8.

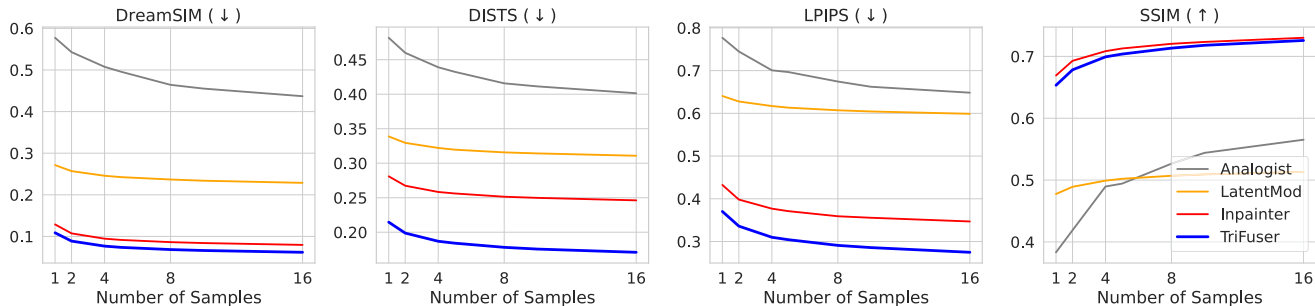


Figure 9. We compare our method, TRIFUSER, against the three baselines with four different metrics. The x-axis of each plot corresponds to the number of samples used for evaluation, demonstration that TRIFUSER remains superior to the baselines across sample count.

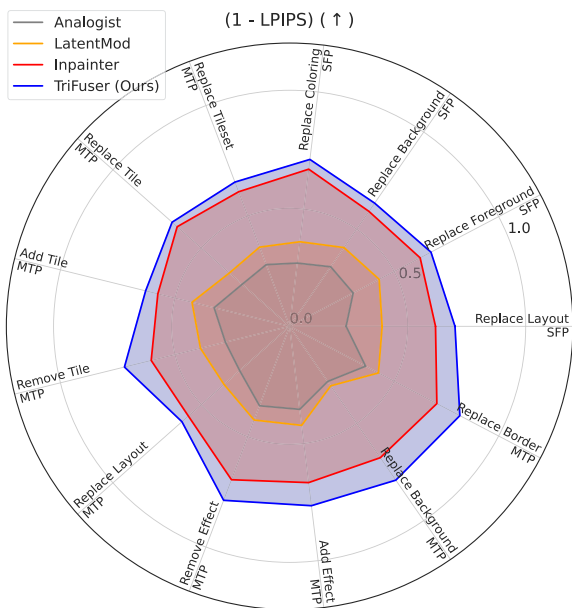


Figure 10. We compare our model against the baselines on a per-edit type basis. We observe that our model obtains higher perceptual similarity to the ground truth target across the edit types.

385 7.1. LatentMod Ablation

386 An important baseline we considered is *LatentMod*, where
 387 first we train a model to learn a latent space for represent-
 388 ing patterns, followed by deploying *latent-arithmetic* [12]
 389 to create analogical patterns. Specifically, we first train a
 390 Image Variation Latent Diffusion Model (LDM) on our pat-
 391 tern dataset (i.e. condition on tokens extracted from a pat-
 392 tern image to denoise the same pattern image). Then, dur-
 393 ing test-time, given patterns (A, A', B) we infer the ana-
 394 logically edited pattern B' by using the LDM to denoise a
 395 Gaussian-initialized latent conditioned on the latent arith-
 396 metic tokens $(E(B) + E(A') - E(A))$. In this section we
 397 explore different variations of this model, demonstrating the
 398 superiority of the baseline used in the main paper over its al-

ternatives.

First, we consider two architectures for the Image vari-
 ation model. The first, referred to as CATEGORICAL, uses
 only a single pooled token (i.e. a 1×768 size embedding)
 as the conditioning input $E(A)$. The second, referred to as
 TOKENWISE, uses all the 257 image tokens generated by
 the token extracted (i.e. a 257×768 size embedding) as
 the conditioning input $E(A)$. Finally, we also consider an al-
 ternative of CATEGORICAL, as introduced in DeepVisualAnal-
 ogy [10]. This variation, referred to as ANALOGICAL, has
 the same architecture as CATEGORICAL, but has an alter-
 nate loss formulation which resembles the test-time usage.
 Essentially, this model is trained to denoise B' while being
 conditioned on $E(B) + E(A') - E(A)$ explicitly. Note that
 CATEGORICAL and TOKENWISE only require a dataset of
 training patterns, whereas ANALOGICAL requires analogi-
 cal quartets (A, A', B, B') during training as well (similar
 to conditional generative approaches like ImageBrush [11]
 and our approach, TRIFUSER).

Table 1 compares these approaches on our synthetic
 validation set, reporting perceptual metrics—DSim [5],
 DIST [4] and LPIPS [16]—along with SSIM to capture
 pixel-level structural similarity. We first note that TO-
 KENWISE shows worse results than CATEGORICAL. Since
 TOKENWISE is conditioned on a large embedding of size
 257×768 , the latent embedding fails to aid analogical
 reasoning (i.e. compression is essential for learning a latent
 space capable of analogical latent arithmetic). Secondly,
 we notice a surprising result that ANALOGICAL, despite be-
 ing trained explicitly trained for analogical editing, is in-
 fact slightly weaker than CATEGORICAL. Visual inspection
 reveals that although ANALOGICAL and CATEGORICAL gen-
 erate similar results, CATEGORICAL often tends to retain
 more aspects of the input pattern B compared to ANALOGI-
 CAL, which consequently sometimes results in a higher per-
 ceptual similarity to the target B' .

Finally, we remark that all these variations remain sig-
 nificantly weaker than the conditional analogical editors.
 This indicates that Latent Arithmetic is perhaps not suit-

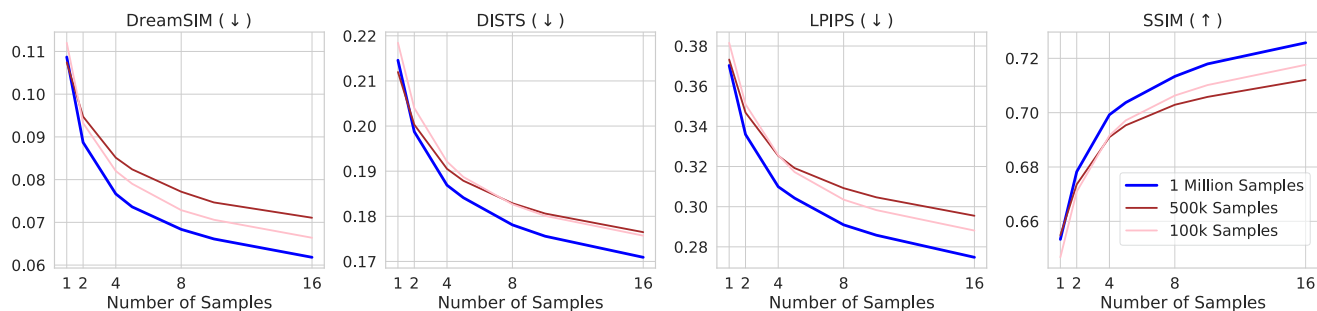


Figure 11. Training TRIFUSER with more analogical quartet samples improves its performance.

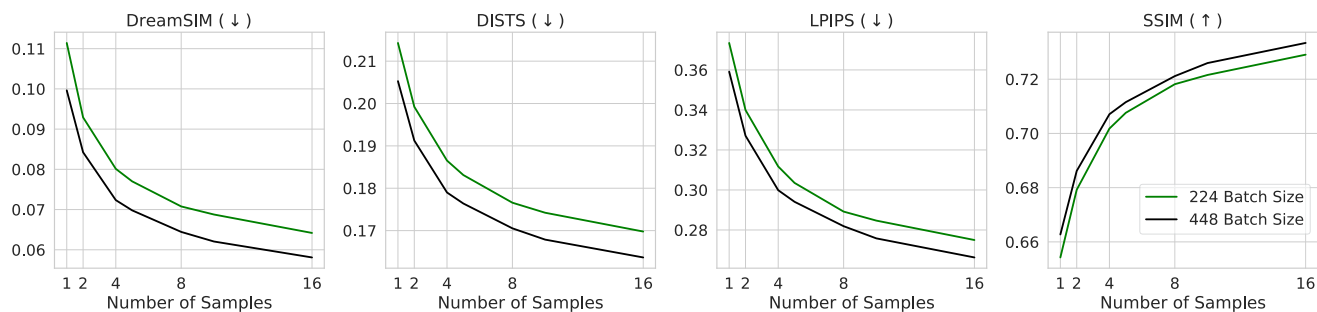


Figure 12. Training TRIFUSER with a larger batch size improves its performance.

438 able for *precise* editing as there is an inherent tussle between
 439 (a) representing sufficient details of patterns in the latent
 440 space to recreate them with high fidelity and (b) having suf-
 441 ficient compression of the latent space to achieve analogical
 442 reasoning via latent arithmetic. Consequently, most image-
 443 editing methods in the diffusion-era have turned towards al-
 444 ternate strategies such as manipulation of attention map [1]
 445 and latent noise inversion [7] for enabling *precise* editing.

446 7.2. TRIFUSER Ablations

447 As described in the main paper, analogies can have multiple
 448 valid interpretations, and even a single interpretation may
 449 yield several visually-related variations. To account for this
 450 multiplicity, we generate k output patterns for each input set
 451 (A, A', B) and select the one that maximizes each metric.
 452 We first elucidate the relation between the number of gener-
 453 ated sample k and the different metrics in Figure 9. We
 454 show four plots, one for each metric. Each plot has the num-
 455 ber of samples k as the x-axis, and the metric (e.g. LPIPS,
 456 SSIM) on the y-axis. These plots reveal that for percep-
 457 tual similarity metrics, TRIFUSER triumphs over the base-
 458 lines across all values of k . Furthermore, as we increase k ,
 459 TRIFUSER significantly closes the gap between itself and
 460 *Inpainter* when measuring SSIM. More importantly, these
 461 plot reveal that using a smaller number of samples ($k = 5$
 462 as used in the main paper) is sufficient, and performance
 463 does not drastically decrease as k is decreased from 16.

We also evaluate all the models separately for each type
 of edit in the synthetic validation set. We measure the average
 $(1 - LPIPS$ with $k = 5)$ (so that higher value indicates
 better performance) for each type of edit and visualize the
 results a radar plot as show in Figure 10. We observe that
 TRIFUSER surpasses all the baselines across the different
 types of edits. For more details regarding the edits, please
 refer to section 5.

472 7.3. TRIFUSER Scalability

473 Recent research has shown that scaling neural approaches,
 474 in terms of computational complexity and dataset size,
 475 is fundamental for achieving compelling results. Conse-
 476 quently, it is critical to investigate the *scalability* of novel
 477 models/methods. In this section, we study the scalability of
 478 TRIFUSER with respect to its training dataset size and its
 479 training compute budget.

480 First, we perform ablations to elicit the relation between
 481 training dataset size and TRIFUSER performance. We train
 482 three variations of TRIFUSER each with a dataset size of
 483 100,000 samples, 500,000 samples and 1 Million samples
 484 respectively. The performance of these three methods is
 485 then compared on the held-out synthetic validation set. The
 486 resulting metrics are visualized as line-plots in Figure 11.
 487 Here, we provide 4 plots, one for each metric, similar to the
 488 format in Figure 9. The x-axis corresponds to the number
 489 of samples (k), and the y-axis corresponds to the respec-

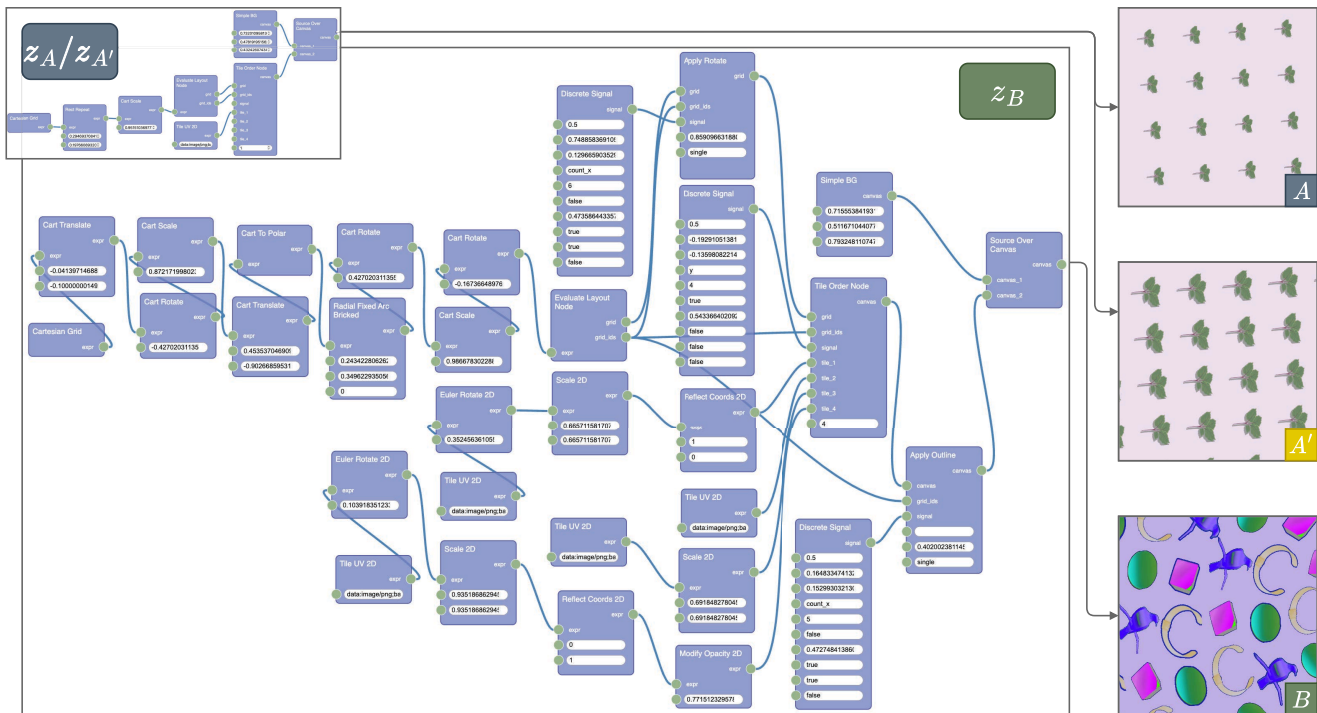


Figure 13. We show an example of a complex synthetic pattern B which has a SPLITWEAVE program z_B with 31 nodes. Inferring such programs automatically, i.e. VPI, is infeasible. Our approach, in contrast, allows to use to construct simple program z_A , and create analogical patterns (A, A') to parametrically edit B , *without* inferring z_B . The task of constructing z_A is significantly easier (in this example, z_A contains 8 nodes, only $\sim 25\%$ of z_B 's size).

490 tive metrics. We notice a meaningful increase in the performance across the different metrics, as we increase the scale
491 of the training dataset. This indicates training the method
492 in future with larger datasets containing even more pattern
493 styles may result in further improvements.
494

495 Similarly, we study the effect of training compute budget
496 on model performance. All our models are typically trained
497 on 8 A100-40GB GPUs with a batch size of 224. To explore
498 the relation between training budget and model performance,
499 we train a variation of TRIFUSER on 8 A100-80GB
500 GPUs with a batch size of 448. We report a comparison
501 between these two models in Figure 12. As shown in this
502 figure, increasing the batch-size results in further improve-
503 ments to the model, indicating a positive correlation w.r.t.
504 the training budget. In future, training TRIFUSER with a
505 larger training budgets may lead to further improvements in
506 the model's performance.

507 8. Qualitative Results

508 We now present qualitative results to emphasize the utility
509 and impressive capabilities of our method. As discussed
510 earlier, a primary motivator for our approach is that Visual
511 Program Inference attempts to infer the a program that fully
512 replicates the input pattern, which not only is a hard task,

but also results in a tedious editing experience as the user of-
513 ten has to fiddle with various parameters to ascertain *which*
514 parts of the program must be edited to attain the desired edit.
515 In contrast, with our approach, the user only has to construct
516 the program for (A, A') which demonstrate *which* property
517 to edit and *how* to edit it. Particularly, A does not need to
518 even be similar to B , making the task of constructing the
519 programs $(z_A, z_{A'})$ considerably simpler.
520

521 In Figure 13, we compare the program of a complex target
522 pattern B , marked as z_B , with the simple program, z_A
523 constructed to create an analogy pair (A, A') for editing the
524 layout of B . While z_B contains 31 operator nodes, z_A
525 contains only 8, which is $\sim 25\%$ of the size of z_B . We make
526 the following notes: (a) The task users need to perform —
527 that of creating z_A — is significantly easier than the task
528 of inferring z_B , (b) Using the analogical editor inducing
529 parametric control over pattern B based on the program z_A .
530 Consequently, to perform simple edits of pattern B , the user
531 only needs to specify a simple program z_A .

532 As mentioned previously, analogies can have multiple
533 valid interpretations, and even a single interpretation may
534 yield several visually-related variations. Consequently, a
535 analogical editor must also be capable of producing mul-
536 tiple interpretations for any given input analogy pairs. Hav-
537 ing such a one-to-many mapping, as our model has, is more

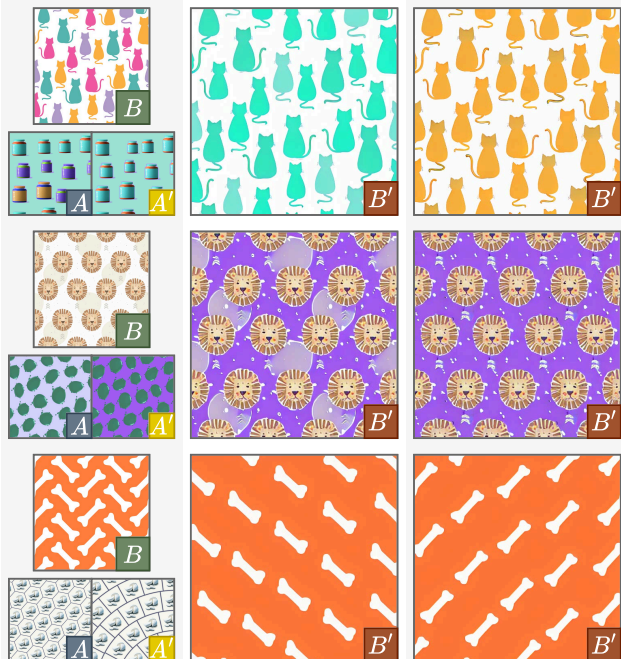


Figure 14. TRIFUSER generates multiple *equally-valid* yet different edited images B' .

suitable for editing as the user can select the edited pattern that matches their edit intent from multiple generations. In contrast, restricting to a singular interpretation may more easily lead to scenarios where the system’s and user’s interpretation of the input analogy differ.

In Figure 14, we present analogical edits performed on real-world patterns by our method, highlighting the generation of different *equally valid* analogy interpretations. The first row corresponds to an edit for removing a random coloring variation effect on the input pattern B . TRIFUSER produces two outcomes, both reasonable as pattern B does not make it clear what the tile’s original color is. The example presented in the second row corresponds to an edit to modify the background of the input pattern. However, it’s unclear if the muted ellipses behind the lion tiles are part of the tile, or part of the background. Consequently, some generations keep these ellipses updating their color accordingly, while other generations eschew them to provide a uniform colored background as shown in A' . Finally, the third example corresponds to an edit on the layout of the input pattern. We show two equally reasonable outputs generated by our model as the underlying orientation of the bone tile is ambiguous.

Finally, in figure 15, we demonstrate the ability of our model to reasonably edit patterns in styles unseen during training. Additionally, we present additional qualitative results comparing our method to the other baselines in Figure 17. Images comparing the four methods across the en-



Figure 15. We present additional examples that show that TRIFUSER effectively edits patterns from novel pattern styles not present in the training dataset.

tire test set is also provided in the supplemental material.

9. Failure Cases

We present and discuss some recurring failure cases for our method. Figure 16 provides 6 examples from our test set of real-world patterns where our method fails to generate a reasonable analogical edit. When editing the layout of patterns, our model still sometimes struggles to retain the fine-details of the input pattern’s tile, particularly when they contain text — this is demonstrated in example (b) and (d). Another mode of failure is when the edit does not *fully* perform the intended edit, as visible in example (c) and (e). In (c) though the model adds a color change effect on B as intended, it produces color variations that do not match the color variations shown in A, A' . This is due to the usage of *relative* color shifts (with respect to a hue-wheel) in our synthetic patterns. Similarly, in (e), while the model correctly removes the tile scaling effect, it replaces the fish tile with the cat tile. Finally, a few failure cases also emerge due to the model failing to understand the input analogy pair, as show in examples (a) and (f).

10. Limitations

While our method demonstrates robust performance and versatility, there are a few limitations that merit discussion.

The primary limitation lies in the reliance on a synthetic dataset of analogies. To extend this technique to other domains, users must construct a domain-specific language (DSL) and define editing functions. Furthermore, real-world applicability of our method depends on the coverage of the DSL and the editing functions. Although we

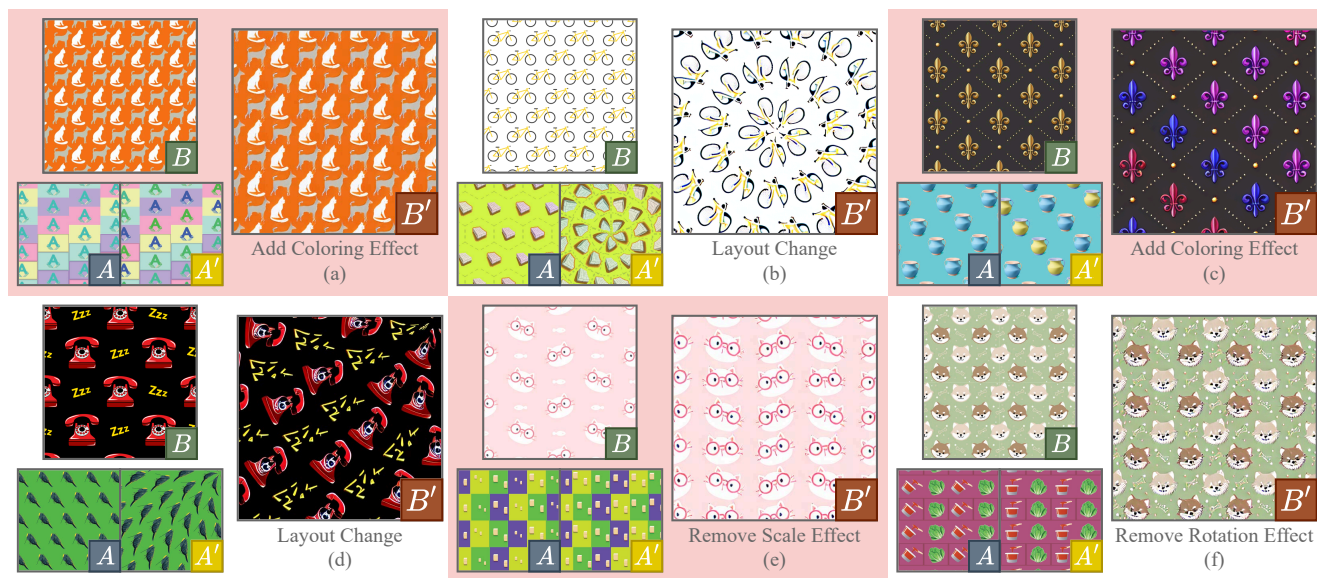


Figure 16. We present examples on the test-set where our method fails to produce a reasonable edit. Edits sometimes fail due to poor retention of tile-details ((b) and (d)), or imperfectly applying the edit demonstrated with (A, A') ((c) and (e)) or failing to understand the input analogy ((a) and (f)).

595 demonstrate generalization to related pattern styles, the cur- 625
 596 rent scale of the dataset limits the model’s ability to han- 626
 597 dle entirely novel pattern styles or edits. However, this 627
 598 limitation may be addressed by automatic the construction 628
 599 of analogical data from multiple domains such as Shader- 629
 600 Toy shader code. Such data could enable pretraining on 630
 601 a broader scope of analogical variations before fine-tuning 631
 602 for specific domains. Additionally, various visual domains 632
 603 such as Zentangle patterns, materials, Lego already contain 633
 604 well defined DSLs making it easier to extend our framework 634
 605 to other structured visual data domains. 635

606 A second drawback is that analogies, while universal in 636
 607 their ability to represent arbitrary edits, are not always the 637
 608 most efficient modality for conveying edit intent. For exam- 638
 609 ple, simple edits such as color changes might be more eas- 639
 610 ily performed through direct recoloring of the canvas. Fur- 640
 611 thermore, the inherent flexibility of analogies, which allows 641
 612 multiple interpretations, can sometimes make it tedious to 642
 613 sample and select a desired output. This issue could be 643
 614 mitigated by coupling analogies with text-based guidance 644
 615 or other constraints to make the process more directed and 645
 616 user-friendly. 646

617 Finally, using the system requires constructing anal- 647
 618 ogy pairs, which depends on the user’s familiarity with 648
 619 SPLITWEAVE or node-based programming. While this 649
 620 could pose a barrier to some users, the increasing adop- 650
 621 tion of node-based tools in visual programming provides 651
 622 a promising path forward. Future research into improving 652
 623 user interaction for visual programming and analogical edit- 653
 624 ing could further lower this barrier and make the system 654

more accessible. 625

626 Despite these limitations, our work provides a flexible 626
 627 framework for analogical pattern editing and highlights sev- 627
 628 eral avenues for future research, including extending ana- 628
 629 logical datasets, improving edit specificity, and enhancing 629
 630 user interfaces. 630



Figure 17. Qualitative comparison between patterns generated by our model, TRIFUSER, and the baselines. TRIFUSER generates higher quality patterns with greater fidelity to the input analogy.

631 **References**

- 632 [1] Yuval Alaluf, Daniel Garibi, Or Patashnik, Hadar Averbuch-
633 Elor, and Daniel Cohen-Or. Cross-image attention for zero-
634 shot appearance transfer. In *ACM SIGGRAPH 2024 Con-*
635 *ference Papers*, New York, NY, USA, 2024. Association for
636 Computing Machinery. 9
- 637 [2] Omer Bar-Tal, Lior Yariv, Yaron Lipman, and Tali Dekel.
638 Multidiffusion: Fusing diffusion paths for controlled image
639 generation. *arXiv preprint arXiv:2302.08113*, 2023. 7
- 640 [3] Rete.js Contributors. Rete.js: Javascript framework for vi-
641 sual programming, 2023. Version 1.x, accessed November
642 20, 2024. 3
- 643 [4] Keyan Ding, Kede Ma, Shiqi Wang, and Eero P. Simoncelli.
644 Image quality assessment: Unifying structure and texture
645 similarity. *CoRR*, abs/2004.07728, 2020. 8
- 646 [5] Stephanie Fu, Netanel Tamir, Shobhita Sundaram, Lucy
647 Chai, Richard Zhang, Tali Dekel, and Phillip Isola. Dream-
648 sim: Learning new dimensions of human visual similarity
649 using synthetic data. *Advances in Neural Information Pro-*
650 *cessing Systems*, 36, 2024. 8
- 651 [6] Dedre Gentner. Structure-mapping: A theoretical framework
652 for analogy. *Cognitive Science*, 7(2):155–170, 1983. 5
- 653 [7] Amir Hertz, Ron Mokady, Jay Tenenbaum, Kfir Aberman,
654 Yael Pritch, and Daniel Cohen-Or. Prompt-to-prompt image
655 editing with cross attention control. 2022. 9
- 656 [8] George A. Miller. WordNet: A lexical database for En-
657 glish. In *Human Language Technology: Proceedings of a*
658 *Workshop held at Plainsboro, New Jersey, March 8-11, 1994*,
659 1994. 4
- 660 [9] Adam Paszke, Sam Gross, Francisco Massa, Adam Lerer,
661 James Bradbury, Gregory Chanan, Trevor Killeen, Zeming
662 Lin, Natalia Gimelshein, Luca Antiga, Alban Desmaison,
663 Andreas Köpf, Edward Yang, Zach DeVito, Martin Raison,
664 Alykhan Tejani, Sasank Chilamkurthy, Benoit Steiner, Lu
665 Fang, Junjie Bai, and Soumith Chintala. *PyTorch: an imper-*
666 *ative style, high-performance deep learning library*. Curran
667 Associates Inc., Red Hook, NY, USA, 2019. 3
- 668 [10] Scott Reed, Yi Zhang, Yuting Zhang, and Honglak Lee. Deep
669 visual analogy-making. In *Proceedings of the 28th Inter-*
670 *national Conference on Neural Information Processing Sys-*
671 *tems - Volume 1*, page 1252–1260, Cambridge, MA, USA,
672 2015. MIT Press. 8
- 673 [11] Yasheng Sun, Yifan Yang, Houwen Peng, Yifei Shen, Yuqing
674 Yang, Han Hu, Lili Qiu, and Hideki Koike. Imagebrush:
675 learning visual in-context instructions for exemplar-based
676 image manipulation. In *Proceedings of the 37th Interna-*
677 *tional Conference on Neural Information Processing Sys-*
678 *tems*, Red Hook, NY, USA, 2024. Curran Associates Inc. 8
- 679 [12] Yoad Tewel, Yoav Shalev, Idan Schwartz, and Lior Wolf.
680 Zero-shot image-to-text generation for visual-semantic arith-
681 metic. *arXiv preprint arXiv:2111.14447*, 2021. 8
- 682 [13] Gregory K. Wallace. The jpeg still picture compression stan-
683 dard. *Commun. ACM*, 34(4):30–44, 1991. 5
- 684 [14] Xiaohua Zhai, Basil Mustafa, Alexander Kolesnikov, and
685 Lucas Beyer. Sigmoid loss for language image pre-training.
686 In *Proceedings of the IEEE/CVF International Conference*
687 *on Computer Vision (ICCV)*, pages 11975–11986, 2023. 4
- [15] Lvmin Zhang and Maneesh Agrawala. Transparent im- 688
age layer diffusion using latent transparency. *ACM Trans.* 689
Graph., 43(4), 2024. 4, 5 690
- [16] Richard Zhang, Phillip Isola, Alexei A Efros, Eli Shechtman, 691
and Oliver Wang. The unreasonable effectiveness of deep 692
features as a perceptual metric. In *CVPR*, 2018. 8 693